www.czasopisma.pan.pl PAN www.journals.pan.pl

ARCHIVES of FOUNDRY ENGINEERING

ISSN (2299-2944)
Volume 2023
Issue 4/2023

105 – 116

10.24425/afe.2023.146685

13/4

Published quarterly as the organ of the Foundry Commission of the Polish Academy of Sciences

Selective Laser Melting Process Parameter Optimization on Density and Corrosion Resistance of 17-4PH Stainless Steel

Priya Sahadevan [a], Chithirai Pon Selvan [b], Manjunath Patel G C [c,*], Amiya Bhaumik [a]

[a] Lincoln University College Selangor, Malaysia
[b] Curtin University Dubai, United Arab Emirates
[c] PES Institute of Technology and Management, Shivamogga, Visvesvaraya Technological University, Belagavi, India
* Corresponding author: E-mail address: manju09mpm05@gmail.com

Received 02.08.2023; accepted in revised form 03.11.2023; available online 22.12.2023

Abstract

The 17-4 PH Stainless Steel material is known for its higher strength and, therefore, extensively used to build structures for aerospace, automotive, biomedical, and energy applications. The parts must operate satisfactorily in different environmental conditions to widen the diverse application. The selective laser melting (SLM) technique build parts cost-effectively, ensuring near-net shape manufacturability. Laser power, scan speed, and hatch distance operating at different conditions were used to develop parts and optimize for higher density in printed parts. Laser power, scan speed, and hatch distance resulted in the percent contribution towards density equal to 73.74%, 24.48%, and 1.78%. The optimized conditions resulted in higher density and relative density equal to 7.76 g/cm^3 and 99.48%. Printed parts' corrosion rate and wear loss showed more stability in NaCl corrosive medium even at 75 ^{o}C than 1M of HCL corrosive medium. Less pitting corrosion was observed on the samples treated in NaCl solution at 25 ^{o}C and 75 ^{o}C at 72 Hrs than in HCL solution. Therefore, 17-4 PH SS parts are best suited even in marine applications.

Keywords: 17-4 PH Stainless Steel, Density, Corrosion studies, SLM

1. Introduction

Corrosion is a naturally occurring process that negatively impacts cost and parts failure (due to the destructive attack of a metal by its chemical reaction with gas, liquid, and solid medium environment) in industry sectors [1, 2]. The metal structures deteriorate in different conditions (parts operating under ambient and elevated temperatures in marine and industrial sectors), resulting in material and economic loss [3-4]. Neglecting marine and structure parts' corrosion resulted in catastrophic failures and financial losses [3]. Economic costs due to corrosion are determined directly (anti-corrosion technologies, namely coatings, monitoring and inspection devices, inhibitors, etc.) and indirectly (parts failure, loss of productivity or efficiency, polluted environment, compensation for repair, etc.) with reliant expertise in corrosion accounts to 3.34% of the gross domestic product in China [1]. The selection of corrosion-inhibiting material is of industrial relevance to limit the detrimental impacts of corrosion.

In recent years, researchers across the globe have explored the corrosion behavior of various metals and alloys subjected to different environments [3, 5-7]. Ferrous metals and alloys are known for their excellent strength, hardness, thermal conductivity, and durability with inadequate corrosion resistance [8]. Nonferrous metals and alloys possess better corrosion resistance with compromising strength, durability, and hardness [9]. Nickel-

based alloys allow easy manufacturability by offering better properties at elevated temperatures in harsh environmental applications [10]. The higher cost of nickel alloys limits a wide range of applications. Iron and its alloys (in particular low alloyed steels) are more susceptible to corrosion and often available at relatively low cost [11]. Stainless steel offers better corrosion resistivity attributed to forming a protective chromium layer [10]. Stainless steels provide better resistance to stress corrosion subjected to a wide range of environments [12]. Better hardness and strength offered by stainless steel showed excellent resistance to erosion corrosion, cavitation, and fatigue corrosion [13]. The proportion of chromium differentiates the grades of steel. The higher chromium content controls the rate of corrosion [14]. Stainless steel (SS) contains approximately 11% chromium, resulting in better corrosion resistance [15]. The precipitate-hardened SS (PHSS) offers 3-4 times higher strength than 304 and 316 SS [16]. Higher strengths and fracture toughness resulting from PHSS ensure such materials are best suited to use in aerospace [17], automotive [18], marine [19], nuclear [20], and medical [21] applications. The PHSS parts are widely applied to load-bearing machine applications in different environments [17]. The 17-4 PH stainless steel provided better mechanical properties, developing engineering structural parts best suited for aerospace, chemical, biomedical, and energy applications [22, 23]. The above literature depicts 17-4 PH stainless steel operating under different environmental conditions to satisfy various applications. Therefore, the corrosion studies of 17-4 PH stainless steels at other ecological conditions and their compatibility with enhanced service life span of industrial parts must be of practical relevance.

In recent years, parts of additive manufacturing (AM) technology have gained rapid momentum in the automotive, aerospace, biomedical, foundry, and construction industries [24]. AM technologies print parts at low cost, possessing (unlike traditional processes: no need to create molds and the ability to fabricate complex geometries in a single processing step) enhanced mechanical properties (might occur because of rapid cooling and solidification) with near net-shaped manufacture capability [24, 25]. Evolution in AM technologies led distinguished researchers across the globe to develop direct energy deposition, binder jetting, and powder bed fusion to print metal parts [26]. DED manufacturers denser quality parts but suffer from poor surface finish, resulting in detrimental effects during their service life [27]. Selective laser melting (SLM) derived based on the powder bed fusion technique produces better quality parts provided the influencing process variables are appropriately controlled [28]. Highly porous parts are probably due to the evaporation of low melting point materials at lower scan speeds and inadequate melting at higher scan speeds [23]. A lower degree of wettability at lower laser power values results in higher porosity [29]. However, higher laser power tends to burn the materials, and the possibility is that the material has a greater tendency to evaporate [28]. Hatch spacing maintained at lower values causes increased overlapping area at the adjacent scanning line tracks, resulting in little thermal influence [30]. The above literature review confirms that additive manufacturing is a cost-effective near-net-shaped technique to print quality parts provided an appropriate control of SLM parameters. There are many research works reported on selection of control variables and their values, viz. classical engineering experiments [22, 23], analytical [31], and design of experimental techniques [28]. The 17-4 PH stainless steel parts (17-4 PHSS) were built with the SLM technique and analyzed the parametric (scan rate, slice depth, and hatch distance) influence on mechanical properties [23]. The energy density influence on porosities and scan strategy on the density of 17-4 PHSS built with the SLM process were studied [32, 33]. The SLM process's optimal conditions are not determined [31-33]. The classical engineering approach study, analyze, and optimize one variable at once and neglects interaction effects, resulting in local solutions [34]. An increase in experimentation costs due to loss of material, time, labor, and energy led researchers to limit the use of classical experiments [35]. Analytical models were established with many assumptions to analyze the heat transfer behavior in building SLM parts [31]. The results of experimental and analytical models vary up to 10-30%, probably due to assumptions made being challenging to meet with practical experiments [31, 36]. DOE limits the conduction of many experimental trials, reducing costs in estimating factor effects that could detail process insights and determine optimal conditions. DOEs were applied to minimize the porosities in AZ31-built parts by controlling the SLM process's technological parameters (scan velocity and laser power) [37]. Taguchi method maximizes the density of Ti6Al4V alloy parts by determining the optimal values of laser power, scan strategy and speed, hatch space, and powder size [38]. DOE technique is applied to optimize the density of AlSiMg0.75 parts by determining the values of laser power, scan speed, and hatch space [39]. Many research works reported on maximizing the density of SLM print parts are primarily due to their direct relationship with microstructure and mechanical properties [39, 40]. The optimized conditions were found to be different for different materials for the following reasons: a) difference in material physical and mechanical properties, b) different melting temperatures, c) different technological parameters analyzed, and d) different experimental and optimization methods. Therefore, optimization for maximum density of 17-4PH SS subjected to SLM technological parameters is of industrial relevance. Taguchi-based DOE is applied to define the experimental matrix, perform parametric analysis, and determine the optimal condition that maximizes the density of 17-4PH SS parts.

The objectives of the proposed work are defined after conducting an extensive literature review:

- Experimental investigation of technological parameters on the performance of SLM-built parts on the density of 17-4PH stainless steel parts.
- Parametric analysis to know the detailed process insights by estimating the factors influencing the density of 17-4PH stainless steel parts.
- Determine optimal conditions that maximize the experimental density of 17-4PH stainless steel parts.
- For the optimized highest density of 17-4 PHSS parts, the corrosion experiments are subjected to different environmental conditions (i.e., acidic and seawater medium at 25, 50, and 75 ^{o}C).
- Recommend the practical utility and environmental compatibility of 17-4 PHSS material applications.

2. Materials and Methodology

2.1. Materials

The 17-4 PH stainless steel material is used to print the parts (dimensions: 10 x 10 x 10 mm) viz. SLM process. The chemical elements of commercially available metal powders (weight % of Cr: 15-17.5, Mo: Max. 0.5, Mn and Si: 1, Ni and Cu: 3-5, Nb: 0.15-0.45) were procured possessing a size of ~50 ± 10 µm. SLM machine (EOSINT M 280) was used to print the cubes of 17-4 PHSS.

2.2. Experimental Variables

The primary parameters critically influencing the density of SLM parts are the laser power, scan speed, layer thickness, beam focus diameter, and hatch distance. Pilot experiments were conducted by varying one-factor-at-a-time at five operating levels and analyzing their effect on density values. The results showed the layer thickness and beam focus diameter do not show maximum variation in the density. The maximum density attained for the corresponding values of layer thickness and beam focus diameter is 40 µm and 100 µm. In addition, the parameters and operating levels are fixed after consulting experts working in industries and literature review [28, 37-39]. The selected machine-related printing parameters, control variables, and levels are presented in Table 1.

2.3. Experimental Method

Taguchi L_9 experimental matrix is employed for three selective laser melting parameters operating at three levels (refer to Table 2). Each experimental condition was repeated thrice and print the 17-4 PHSS parts. The samples were developed using an SLM process. The machine is supplied with laser fiber and has a wavelength of 1083 nm. The continuous laser spot size was about 100 µm throughout the experiment. The SLM method was conducted in a vacuum to prevent the samples from oxidizing. The chamber pressure was kept to $5x10^{-3}$ Pa. In addition, the Argon gas flow was introduced to the experimental setup to review the impact of the climatic conditions on the build quality. The chamber was exhausted by the pressure mentioned. After that, the chamber pressure was adjusted to $1x10^{3}$ Pa using Ar gas to get the flow throughout the optical maser irradiation. The experimental setup is illustrated in Fig. 1, and the method parameters are listed in Table 1.

Table 1.
Variables and operating levels of SLM process

Details	Variable name	Levels (1, 2, 3)
Control parameters	A: Laser power, W	240, 270, 300 W
	B: Scan speed, mm/s	600, 800, 1000 mm/s
	C: Hatch distance, mm	0.08, 0.10, 0.12 mm
Fixed parameters	Laser spot diameter, mm	0.2 mm
	Operational Beam Focus, µm	100
	Minimum Scan Line, µm	100 µm
	Layer thickness, µm	40 µm

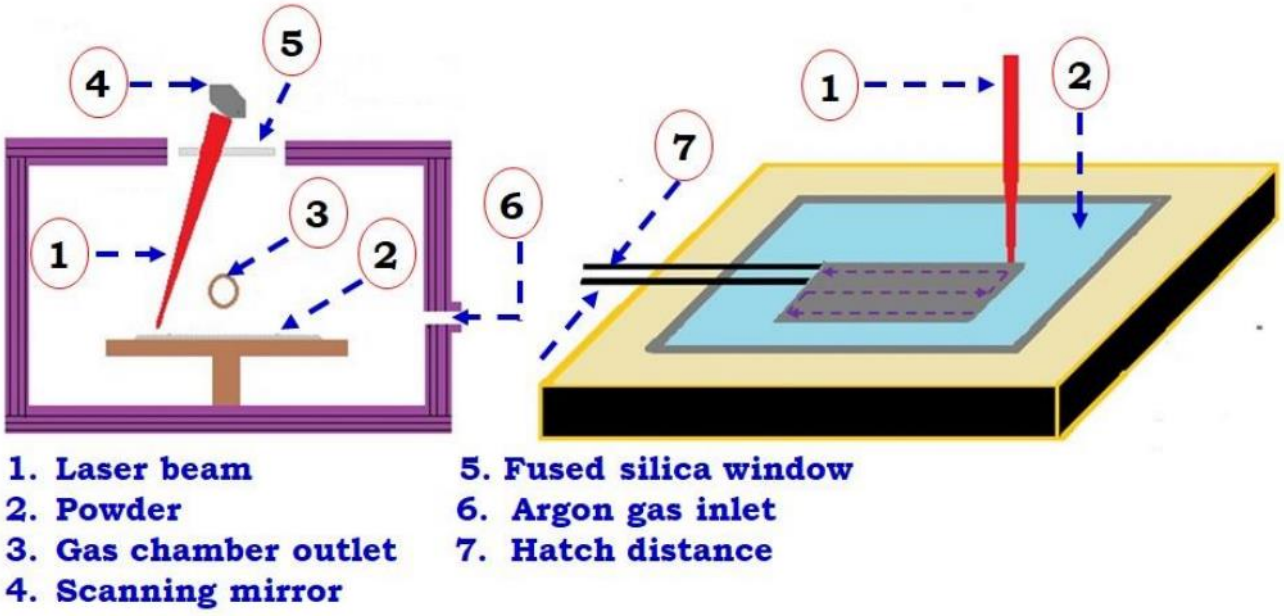

Fig. 1. Representation sketch of SLM Process and its scanning pattern

2.4. Response measurements

The SLM printed parts were subjected to quality examination, such as density and corrosion rate. The details of density and corrosion rate measurements are presented below.

2.4.1. Density Measurement

The density of each printed part was measured using the Archimedes principle. Fig. 2 shows the density measurement kit used to record the density values. The samples used for density measurements are presented in Fig. 3a. The average density values of three 17-4 PHSS printed parts were recorded for parametric analysis and optimization. The computation corresponds to measuring the density of the SLM parts is done by using Eq. 1.

$$\rho_{17-4\ PHSS} = \frac{Density\ of\ water\ -\ Mass\ in\ air}{Mass\ in\ air - Mass\ in\ water} = \frac{g}{cm^3} \quad (1)$$

Note that, the ρ_{Water} is 1 gm/cm^3. The average density values of three replicates correspond to each experimental conditions is presented in Table 2. The theoretical density of 17-4 PH stainless steel is 7.8 g/cm^3. The relative density can be calculated using the Eq. 2.

$$\text{Re}\,lative\ Density\ (\%) = \frac{Measured\ \text{density}}{Theoritical\ \text{density}} \quad (2)$$

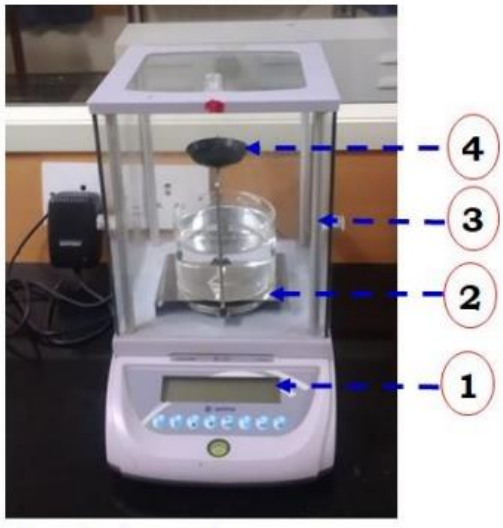

Fig. 2. Density measuring kit

2.4.2. Corrosion rate measurements

Fig. 3b shows the sample used for the corrosion test. The weight loss measurement is the simple technique for quantification of corrosion rate. ASTM G1-90 standards were

used to measure the weight loss under different conditions (acidic medium: 1M of HCL, and 3% of NaCl medium stimulating seawater conditions). Prior to weight loss measurement, all the printed samples were cleaned with deionized water, followed by acetone and air drying. The weight of dried samples is recorded with a Sartorius electronic digital weighing balance (sensitivity of 0.1 mg). The dried samples were weighed after immersion in a corrosive medium subjected to different temperatures such as 25, 50, and 75 ºC. Record the weight of samples immersed in a corrosive medium. The weight of samples was measured at different periodic intervals of 24, 48, and 72 hours. The weight loss was calculated for every sample at regular intervals after carefully cleaning and drying. The pH of the corrosive medium solution was recorded before and after the experimentation with the help of Systronics Digital pH meter 335. The weight loss and corrosion rate were computed using Eq. 3 and 4 [41, 42].

$$Weight\ Loss\ (\%) = \frac{Weight\ loss\ after\ \exp erimentation}{Initial\ weight\ of\ the\ sample} \tag{3}$$

$$Corrossion\ rate\ (mm/y) = \frac{K \times W}{D \times A \times T} = \frac{8.76 \times 10^4 \times Weight\ Loss\ (g)}{Alloy\ density\ (g/cm^3) \times Exposed\ area\ (cm^2) \times Exposure\ time\ (h)} \tag{4}$$

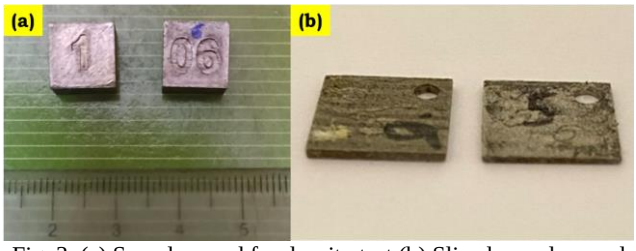

Fig. 3. (a) Samples used for density test (b) Sliced samples used for corrosion test.

3. Result and Discussion

The results of this research work are presented and discussed in two folds: 1. Experimental data analysis and optimization of density of 17-4 PHSS parts. 2. Corrosion studies for the obtained higher-density parts at different environmental conditions.

3.1. Experimental Data Collection and Analysis

Taguchi L_9 experiments with the different combinations of SLM parameters were carried out and collected the input-output data. The average values of three density results correspond to each experimental condition with deviation from the mean value is presented in Table 2. The actual density is transformed to signal-to-noise ratio (S/N) to maximize the better-quality characteristics using Eq. 5.

$$S/N\ ratio\ _{\rho} = \eta_{ij} = -10Log\left(\frac{1}{n}\sum\nolimits_{i=1}^{n}\frac{1}{y_{ij}^2}\right) \tag{5}$$

n = 1, 2,.....m; j = 1, 2,.....p

The computation of S/N ratio (η_{ij}) correspond to each experimental trial (say i^{th}) correspond to jth output. The computed S/N ratio values is presented in Table 2.

Table 2.
Input-output data of SLM process

Exp. No.	Input variables in coded (uncoded)			Output variable	
	A, W	B, mm/s	C, mm	Density, g/cm^3	Signal-to-noise ratio (dB)
1-17-4 PHSS	1(240)	1(600)	1(0.08)	7.28 ± 0.03	17.24
2-17-4 PHSS	1(240)	2(800)	2(0.1)	7.32 ± 0.04	17.29
3-17-4 PHSS	1(240)	3(1000)	3(0.12)	7.39 ± 0.03	17.37
4-17-4 PHSS	2(270)	1(600)	2(0.1)	7.45 ± 0.02	17.44
5-17-4 PHSS	2(270)	2(800)	3(0.12)	7.47 ± 0.03	17.47
6-17-4 PHSS	2(270)	3(1000)	1(0.08)	7.65 ± 0.02	17.67
7-17-4 PHSS	3(300)	1(600)	3(0.12)	7.54 ± 0.03	17.55
8-17-4 PHSS	3(300)	2(800)	1(0.08)	7.61 ± 0.04	17.63
9-17-4 PHSS	3(300)	3(1000)	2(0.1)	7.74 ± 0.02	17.77

3.2. Analysis of factors using Pareto ANOVA

Pareto analysis of variance is conducted to determine the factor contribution and optimal condition towards individual output. The S/N ratio corresponding to density values was used for factor analysis and optimization. The sum at each level for a factor is determined to examine the factor effects on S/N ratio values of density. The percent contribution for a factor that influences the density is computed based on the sum of squares of differences. The highest values correspond to the sum at factor levels and were identified as the optimal level for that factor. The results of the Pareto analysis of variance are presented in Table 3.

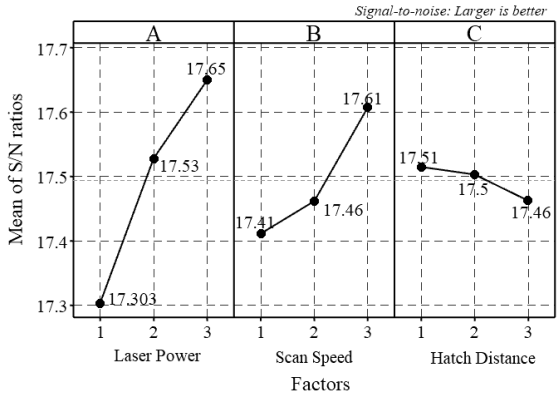

Fig. 4. Main effect plot for density

The factors operating at three levels and their mean values (based on the sum at factor levels) were used to determine the individual effects on the density (refer to Fig. 4). Increase in laser power and scan speed was found to increase the density of 17-4 PHSS. Low laser power and scan speed values do not have sufficient energy density to melt all metal powders, resulting in discontinuities or voids in 17-4 PHSS parts [43, 44]. The discontinuities in the metal-printed parts lower the density values [45]. Note that low values of scan speed require the SLM machine to operate at a higher operating temperature that ensures the melting of all metal powders. In addition, low scan speed and laser power values resulting in low melting temperature (due to low energy density) cause un-melted regions, leading to voids forming in the printed parts [43]. Higher laser power and scan speed result in higher energy density that causes melting of all the metal powders, ensuring better fusion characteristics between the metal powders [46]. Hatch distance maintained at low values causes increased overlap adjacent to scan lines. The higher energy distributions between the scan lines tend to melt all metal powders and flow on already solidified scanning lines resulting in strong hard-surface layers [28]. High values of hatch distance tend to lower the energy density, resulting in less or no overlap between the hatch lines or tracks [47]. Higher hatch distance tends to minimize the overlap that could reduce the melt pool's wettable and thermal conduction characteristics [48, 49]. In addition, higher hatch spacing fails to wet the surrounding or previous layer by molten metal, which causes insulating metal powders, and slower cooling characteristics enable surface tension effects to cause pores or voids [50, 51]. The defects (lack of melt pool overlap and melt pool discontinuities) between the layers of the printed parts lower the density in 17-4 PHSS parts [48]. The negligible variations in hatch distance were also observed in recent literature [28-30]. Note that the laser power, scan speed, and hatch distance mean values of density (computed based on S/N ratio) from level 1 to level 3 varied linearly from 17.30 to 17.65, 17.41 to 17.61 and 17.51 to 17.46, respectively. The percent contribution (computed based on the sum of squares of differences and sum at factor levels) corresponding to each factor on density is found to equal 73.74% for laser power, 24.48% for scan speed, and 1.78% for hatch distance, respectively (refer Table 3).

Table 3.
Results of pareto analysis of variance for density

Factors	Levels	Laser power	Scan speed	Hatch distance	Total
Sum at Factor Levels	1	51.91	52.23	52.54	157.44
	2	52.58	52.38	52.51	
	3	52.95	52.82	52.39	
Sum of square of differences		1.68	0.56	0.04	2.283
Percent contribution		73.74	24.48	1.78	100.00
Parameter optimal condition: $A_3B_3C_1$: Laser power, scan speed, and hatch distance: 300 W, 1000 mm/s, and 0.08 mm					

3.3. Optimization for highest density

The optimal conditions determined are not the set of L_9 experimental matrix, and thus obtained probably due to the multi-factor nature of nine experiments conducted instead of 27. The optimal conditions that maximize the density with the laser power, scan speed, and hatch distance parameters set at 300 W, 1000 mm/s, and 0.08 mm equal 7.76 g/cm^3 (refer Table 3). The optimal conditions (higher laser and scan speed and lower hatch distance) were similar to those obtained earlier by authors' published research works [28, 50]. The energy density corresponds to optimal conditions that maximize the density, equal to 93.75 J/mm^3. The relative density of 17-4 PHSS parts corresponding to optimal conditions equals 99.48%.

3.4. Corrosion Studies

The optimized SLM conditions (laser power, scan speed, and hatch distance: 300 W, 1000 mm/s, and 0.08 mm) resulted in the highest density (i.e., 7.76 g/cm^3) in printed parts used to perform the corrosion studies. Three replicate experiments were performed for the optimized condition. The corrosion studies were conducted on the optimized conditioned samples at both acidic and marine (NaCl medium stimulating the sea water) environments with a time span of up to 72 hours (three intervals with a step size of 24 hours). Furthermore, similar experiments were carried out for temperatures equal to 25, 50, and 75 ^{o}C. The average three values corresponding to weight loss and corrosion rate are presented in Table 4.

Table 4.
Corrosion study results at different environments

Temperature	Corrosion medium	Weight of the sample before the experiment	Weight of the sample after the experiment	Weight loss (mg)	Time (hrs)	Corrosion rate: KW/DAT	Weight loss (%)
25	HCL	0.7125	0.6888	23.7	24	5.58	3.33
		0.7125	0.6611	31.4	48	6.05	7.21
		0.7125	0.5632	31.4	72	11.72	20.95
50	HCL	0.6337	0.6001	91.5	24	7.91	5.30
		0.6337	0.5632	133.5	48	8.30	11.13
		0.6337	0.4002	133.5	72	18.33	36.85
75	HCL	0.6341	0.3353	394.3	24	70.36	47.12
		0.6341	0.2498	551.2	48	45.25	60.61
		0.6341	0.0929	551.2	72	42.48	85.35
25	NaCl	0.7193	0.719	0.3	24	0.071	0.042
		0.7193	0.7186	0.7	48	0.082	0.097
		0.7193	0.7177	1.6	72	0.126	0.222
50	NaCl	0.7102	0.7007	9.5	24	2.24	1.34
		0.7102	0.6955	10.1	48	1.73	2.07
		0.7102	0.6868	23.4	72	1.84	3.29
75	NaCl	0.7159	0.7045	11.4	24	2.68	1.59
		0.7159	0.6985	20.4	48	2.05	2.43
		0.7159	0.6883	25.6	72	2.17	3.86

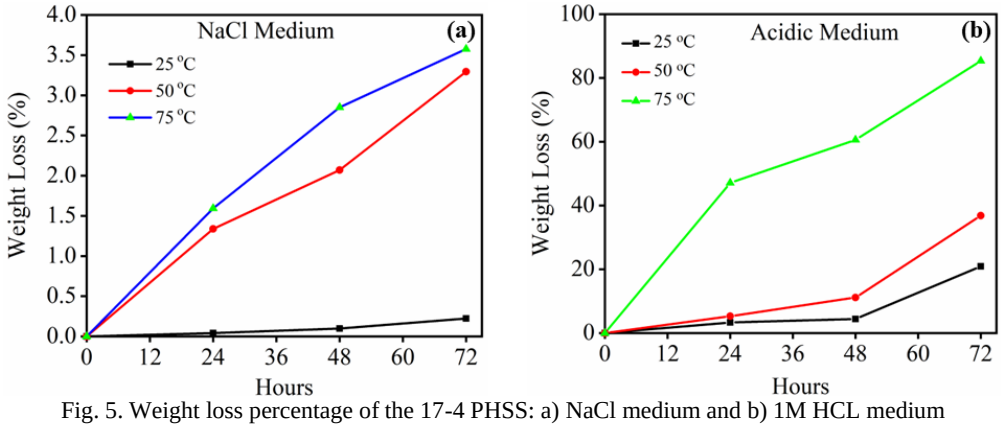

Fig. 5. Weight loss percentage of the 17-4 PHSS: a) NaCl medium and b) 1M HCL medium

Fig. 5 illustrate the weight loss behaviour of 17-4 PHSS at different corrosive medium and temperature (25-75 ^{o}C). The 17-4 PHSS parts showed greater resistance to NaCl corrosive medium even at higher temperatures, i.e., 75 ^{o}C. The metal parts quickly lose weight in a 1M HCL corrosive medium at all temperatures. However, the printed parts undergo a rapid increase in corrosion behaviour with higher temperatures.

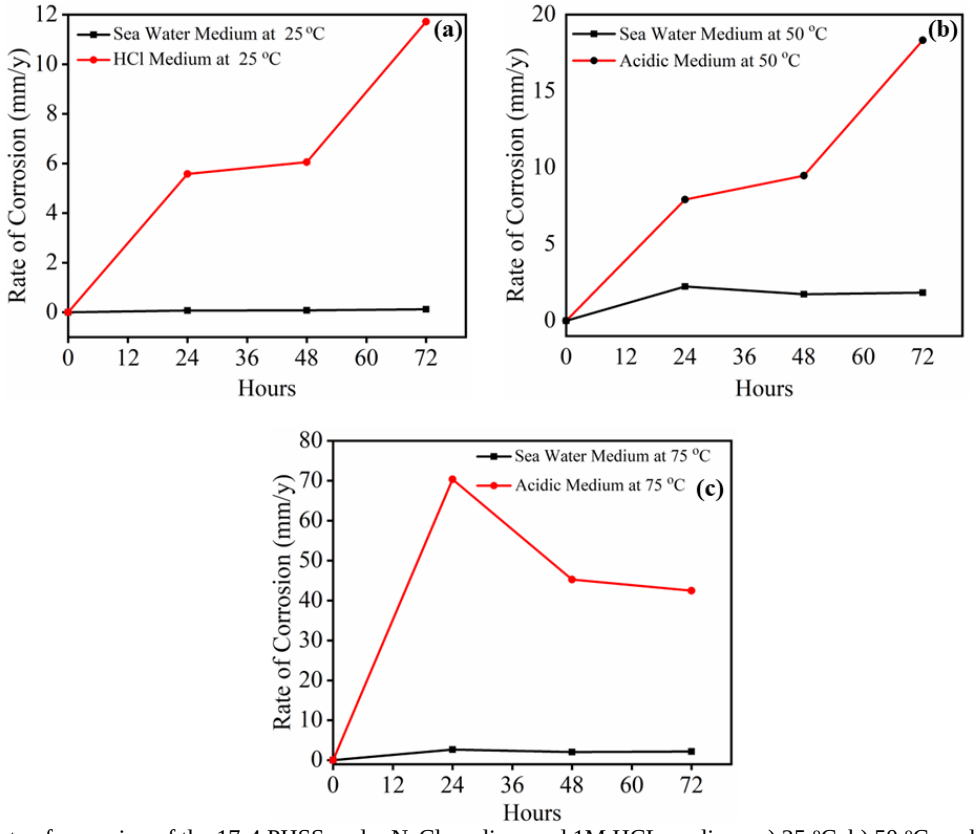

Fig. 6. Rate of corrosion of the 17-4 PHSS under NaCl medium and 1M HCL medium: a) 25 °C, b) 50 °C, and c) 75 °C

Fig. 6a-c shows the corrosion rate of 17-4PHSS parts at different temperatures, and a corrosive medium is presented. Fig. 6a illustrates the corrosion rate in two extremely corrosive mediums at 25°C. The result shows that the corrosion rate in seawater and acidic medium after the 24 hrs of immersion of samples is found equal to 0.070645 x 10^{-2} mm/y and 0.125591 mm/y. The printed metal undergoes extensive corrosion in an acidic medium and rises to 11 mm/y after 72 hours. Similar variations with more corrosion rate were observed with higher temperatures (refer Fig. 6b-c). This indicates that the 17-4PHSS is best suited to operate under marine environmental conditions, even at higher temperatures. The presence of 15-17.5% of Cr could protect the material (by forming a thin passive layer) from corrosion attack. The passive thin surface film ensures a protective blanket to the metal surface, decreasing the corrosion rate and developing probable growth rates of protective layers. This probably retard the deterioration of printed metals over a period of time. Therefore, the 17-4PHSS parts are highly resistant to extreme saline conditions.

In an acidic medium, the material deterioration is higher, probably due to the strong dissolution of metal in 1M HCL. The 1M HCL is a strong oxidizing agent, resulting in electrochemical solid reactions between the metal and acidic medium. The available oxygen and corrosive medium will form a corrosion cell with the metal atoms and initiate the corrosion process. This results in a strong corrosion current, which triggers the electrochemical reaction. The chemical reaction resulted in the formation of ferric chloride, which further oxidizes to ferric oxide and causes rust. The corrosion products formed here are unstable and do not adhere to the metal surface as they dissolve in an acidic medium. This phenomenon is known as chloride aggressiveness, which finally results in the complete deterioration of the metal in an acidic medium. Therefore, the 17-4PHSS fabricated metal parts are not suitable for acidic corrosive environments.

Fig. 7 displays the SEM morphology of 17-4PH SS under various mediums. Fig. 7 (a) and (b) show the SEM morphology of 17-4PH SS at 25 °C and 75 °C in HCL as a corrosive medium. Fig. 7 (c) and (d) show the SEM morphology of 17-4PH SS at 25 °C and 75 °C in NaCl as a corrosive medium. From Fig. 7(a) and 7(c), we can observe there is moderate corrosion at 25 °C at 72 Hrs in both HCL and NaCl mediums than that of Fig. 7(b) and 7(d) at 75 °C at 72 Hrs in both HCL and NaCl mediums.

Also, various corrosion characteristics such as cracks, pits, and high and moderate corrosion areas can be found in the SEM micrographs. Compared to Figs. 7(c) and 7(d), Figs. 7(a) and 7(b) display more pits and corroded surface. Overall, it can be noted that these pits were attributed to chemical dissimilarities around the melt pool boundaries and matched the prevalent symmetry of the melt pools. The overall density of detectable pitting was significantly lower in the NaCl samples, compared to that of HCl samples, after immersion in the HCl solution. Similar observations were noticed by Cabezon et al. [51].

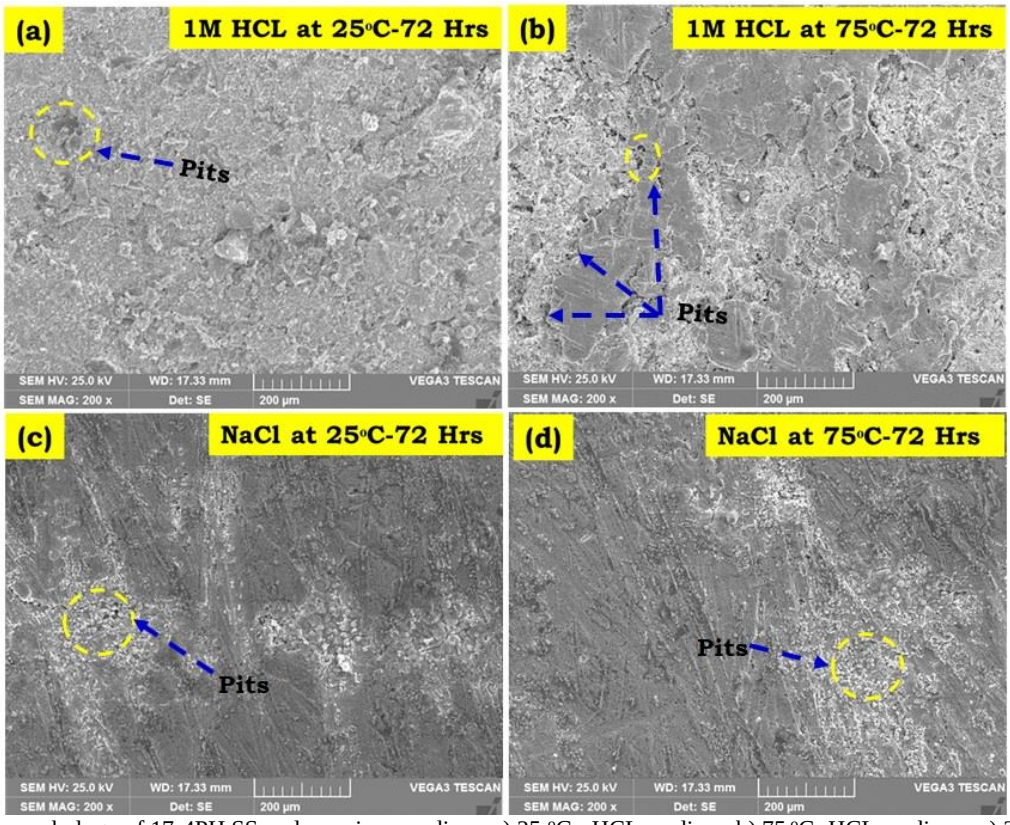

Fig. 7. SEM morphology of 17-4PH SS under various medium: a) 25 ºC. -HCL medium. b) 75 ºC -HCL medium. c) 25 ºC. -NaCl medium. and d) 75 ºC. -NaCl medium at 300 W, 1000 mm/sec and 0.08 mm

4. Conclusions

The following conclusions are drawn as follows:

1. The cost-effective Taguchi L_9 experimental matrix is applied to analyze and optimize the process variables such as laser power, scan speed, and hatch distance on the density of 17-PHSS parts.
2. Laser power, scan speed, and hatch distance percent contribution on density equals 73.74%, 24.48%, and 1.78%, respectively.
3. The optimal conditions are determined for the highest density, viz., Pareto analysis of variance. The optimal conditions were found to be the laser power, scan speed, and hatch distance equal to 300 W, 1000 mm/s, and 0.08 mm. Note that optimal conditions are not from the set of L_9 experiments and are determined by statistical analysis without much experimentation.
4. The optimal conditions generate a higher energy density equal to 93.75 J/mm^3. The higher energy density generates highly intense heat to melt all metal powders and fuse between metal powders, ensuring strong bonding. The relative density (measured/theoretical) of 17-4 PHSS parts corresponding to optimal conditions equals 99.48%.
5. The corrosion study experiments (at different corrosive mediums and temperatures) were conducted on the parts printed with the highest density corresponding to optimal conditions. The samples immersed in NaCl medium resulted in lesser weight loss and corrosion rate at all temperatures than in 1M HCL medium. This suggests the 17-4 PHSS parts best suit the marine applications.
6. Less pitting was observed in micrographs immersed in NaCl solution at 25 ºC. and 75 ºC at 72 Hrs, respectively, compared to that of HCL medium. Also, various corrosion characteristics, such as cracks and pits, were found in the SEM micrographs.
7. The research work can be extended by conducting experiments viz. central composite design. Thereby, interaction effects and empirical predictive equations can be established. Furthermore, applying artificial intelligence algorithms ensures determining the global optimal solutions for density and corrosion. The authors are currently working in the said directions.

References

[1] Hou, B., Li, X., Ma, X., Du, C., Zhang, M., Zheng, M., Xu, W., Lu, D. & Ma, F. (2017). The cost of corrosion in China. *Materials Degradation.* 1(1), 4. DOI:10.1038/s41529-017-0005-2.

[2] Khan, M.A.A., Hussain, M. & Djavanroodi, F. (2021). Microbiologically influenced corrosion in oil and gas

industries: A review. *International Journal of Corrosion and Scale Inhibition.* 10(1), 80-106. DOI: 10.17675/2305-6894-2021-10-1-5.

[3] Bhandari, J., Khan, F., Abbassi, R., Garaniya, V. & Ojeda, R. (2015). Modelling of pitting corrosion in marine and offshore steel structures–A technical review. *Journal of Loss Prevention in the Process Industries.* 37, 39-62. https://doi.org/10.1016/j.jlp.2015.06.008.

[4] Abbas, M. & Shafiee, M. (2020). An overview of maintenance management strategies for corroded steel structures in extreme marine environments. *Marine Structures*. 71, 102718. https://doi.org/10.1016/j.marstruc.2020.102718.

[5] Chalisgaonkar, R. (2020). Insight in applications, manufacturing and corrosion behaviour of magnesium and its alloys–A review. *Materials Today: Proceedings*. 26, 1060-1071. https://doi.org/10.1016/j.matpr.2020.02.211.

[6] Zhu, J., Li, D., Chang, W., Wang, Z., Hu, L., Zhang, Y., & Zhang, L. (2020). In situ marine exposure study on corrosion behaviors of five alloys in coastal waters of western Pacific Ocean. *Journal of Materials Research and Technology*. 9(4), 8104-8116. https://doi.org/10.1016/j.jmrt.2020.05.060.

[7] Swamy, P.K., Mylaraiah, S., Gowdru Chandrashekarappa, M.P., Lakshmikanthan, A., Pimenov, D.Y., Giasin, K. & Krishna, M. (2021). Corrosion behaviour of high-strength Al 7005 alloy and its composites reinforced with industrial waste-based fly ash and glass fibre: comparison of stir cast and extrusion conditions. *Materials*. 14(14), 3929. https://doi.org/10.3390/ma14143929.

[8] Varol, T., Güler, O., Yıldız, F. & Suresh Kumar, S. (2022). Additive manufacturing of non-ferrous metals. *In Innovations in Additive Manufacturing.* (pp. 91-120). Cham: Springer International Publishing. https://doi.org/10.1007/978-3-030-89401-6_5.

[9] Mahmoodian, M. (2018). Introduction. In: *Reliability and maintainability of in-service pipelines*. India: Elsevier.

[10] Ssenteza, V., Eklund, J., Hanif, I., Liske, J. & Jonsson, T. (2023). High temperature corrosion resistance of FeCr (Ni, Al) alloys as bulk/overlay weld coatings in the presence of KCl at 600° C. *Corrosion Science*. 213, 110896. https://doi.org/10.1016/j.corsci.2022.110896.

[11] Folkeson, N., Jonsson, T., Halvarsson, M., Johansson, L.G. & Svensson, J.E. (2011). The influence of small amounts of KCl (s) on the high temperature corrosion of a Fe-2.25 Cr-1Mo steel at 400 and 500° C. *Materials and Corrosion*. 62(7), 606-615. https://doi.org/10.1002/maco.201005942.

[12] Müller, P., Pernica, V. & Kaňa, V. (2022). Corrosion resistance of cast duplex steels. *Archives of Foundry Engineering*, 22(3), 5-10. DOI: 10.24425/afe.2022.140230.

[13] Francis, R. & Byrne, G. (2018). The erosion corrosion limits of duplex stainless steels. *Materials Performance.* 57(5), 44-47.

[14] Sahu, S., Swanson, O.J., Li, T., Gerard, A.Y., Scully, J.R. & Frankel, G.S. (2020). Localized corrosion behavior of non-equiatomic NiFeCrMnCo multi-principal element alloys. *Electrochimica acta*. 354, 136749. https://doi.org/10.1016/j.electacta.2020.136749.

[15] Chen, H., Kim, S.H., Kim, C. Chen, J. & Jang, C. (2019). Corrosion behaviors of four stainless steels with similar chromium content in supercritical carbon dioxide environment at 650 C. *Corrosion Science.* 156, 16-31. https://doi.org/10.1016/j.corsci.2019.04.043.

[16] Zai, L., Zhang, C., Wang, Y., Guo, W., Wellmann, D., Tong, X. & Tian, Y. (2020). Laser powder bed fusion of precipitation-hardened martensitic stainless steels: a review. *Metals.* 10(2), 255. https://doi.org/10.3390/met10020255.

[17] Li, J., Zhan, D., Jiang, Z., Zhang, H., Yang, Y. & Zhang, Y. (2023). Progress on improving strength-toughness of ultra-high strength martensitic steels for aerospace applications: a review. *Journal of Materials Research and Technology*. 23, 172-190. https://doi.org/10.1016/j.jmrt.2022.12.177.

[18] Davanageri, M., Narendranath, S. & Kadoli, R. (2016). Dry sliding wear behavior of super duplex stainless steel AISI 2507: A statistical approach. *Archives of Foundry Engineering.* 16(4), 47-56.

[19] Ghaffari, M., Nemani, A. V. & Nasiri, A. (2022). Microstructure and mechanical behavior of PH 13–8Mo martensitic stainless steel fabricated by wire arc additive manufacturing. *Additive Manufacturing.* 49, 102374. https://doi.org/10.1016/j.addma.2021.102374.

[20] Alım, B., Özpolat, Ö.F., Şakar, E., Han, İ., Arslan, İ., Singh, V.P. & Demir, L. (2022). Precipitation-hardening stainless steels: Potential use radiation shielding materials. *Radiation Physics and Chemistry*. 194, 110009. https://doi.org/10.1016/j.radphyschem.2022.110009.

[21] Yeganeh, M., Shoushtari, M.T. & Jalali, P. (2021). Evaluation of the corrosion performance of selective laser melted 17-4 precipitation hardening stainless steel in Ringer's solution. *Journal of Laser Applications*. 33(4). https://doi.org/10.2351/7.0000445.

[22] Rafi, H.K., Pal, D., Patil, N., Starr, T.L. & Stucker, B.E. (2014). Microstructure and mechanical behavior of 17-4 precipitation hardenable steel processed by selective laser melting. *Journal of materials engineering and performance*. 23, 4421-4428. https://doi.org/10.1007/s11665-014-1226-y.

[23] Hu, Z., Zhu, H., Zhang, H. & Zeng, X. (2017). Experimental investigation on selective laser melting of 17-4PH stainless steel. *Optics & Laser Technology*. 87, 17-25. https://doi.org/10.1016/j.optlastec.2016.07.012.

[24] Srivastava, M., Rathee, S., Tiwari, A. & Dongre, M. (2023). Wire arc additive manufacturing of metals: A review on processes, materials and their behaviour. *Materials Chemistry and Physics*. 294, 126988. https://doi.org/10.1016/j.matchemphys.2022.126988.

[25] Piekło, J. & Garbacz-Klempka, A. (2021). Use of selective laser melting (SLM) as a replacement for pressure die casting technology for the production of automotive casting. *Archives of Foundry Engineering.* 21(2), 9-16. DOI: 10.24425/afe.2021.136092.

[26] Fuchs, S.L., Praegla, P.M., Cyron, C.J., Wall, W.A. & Meier, C. (2022). A versatile SPH modeling framework for coupled microfluid-powder dynamics in additive manufacturing: binder jetting, material jetting, directed energy deposition and powder bed fusion. *Engineering with Computers.* 38(6), 4853-4877. https://doi.org/10.1007/s00366-022-01724-4.

[27] Zhu, Y.Y., Tang, H.B., Li, Z., Xu, C. & He, B. (2019). Solidification behavior and grain morphology of laser additive manufacturing titanium alloys. *Journal of Alloys*

and Compounds. 777, 712-716. https://doi.org/10.1016/j.jallcom.2018.11.055.
[28] Sheshadri, R., Nagaraj, M., Lakshmikanthan, A., Chandrashekarappa, M.P.G., Pimenov, D.Y., Giasin, K., & Wojciechowski, S. (2021). Experimental investigation of selective laser melting parameters for higher surface quality and microhardness properties: Taguchi and super ranking concept approaches. *Journal of Materials Research and Technology*, 14, 2586-2600. https://doi.org/10.1016/j.jmrt.2021.07.144.
[29] Li, R., Shi, Y., Wang, Z., Wang, L., Liu, J. & Jiang, W. (2010). Densification behavior of gas and water atomized 316L stainless steel powder during selective laser melting. *Applied Surface Science*. 256(13), 4350-4356. https://doi.org/10.1016/j.apsusc.2010.02.030.
[30] Averyanova, M., Cicala, E., Bertrand, P., Grevey, D. (2012). Experimental design approach to optimize selective laser melting of martensitic 17-4 PH powder: part I single laser tracks and first layer. *Rapid Prototyping Journal.* 18(1), 28e37. https://doi.org/ 10.1108/13552541211193476
[31] Razavykia, A., Brusa, E., Delprete, C. & Yavari, R. (2020). An overview of additive manufacturing technologies—a review to technical synthesis in numerical study of selective laser melting. *Materials.* 13(17), 3895. https://doi.org/10.3390/ma13173895.
[32] Gu, H., Gong, H., Pal, D., Rafi, K., Starr, T., Stucker B, Influences of energy density on porosity and microstructure of selective laser melted 17-4PH stainless steel. *In 2013 International Solid Freeform Fabrication Symposium*. University of Texas at Austin, 2013-August.
[33] Rashid, R., Masood, S.H., Ruan, D., Palanisamy, S., Rashid, R.R. & Brandt, M. (2017). Effect of scan strategy on density and metallurgical properties of 17-4PH parts printed by Selective Laser Melting (SLM). *Journal of Materials Processing Technology.* 249, 502-511. https://doi.org/10.1016/j.jmatprotec.2017.06.023.
[34] Weissman, S.A. & Anderson, N.G. (2015). Design of experiments (DoE) and process optimization. A review of recent publications. *Organic Process Research & Development.* 19(11), 1605-1633. https://doi.org/10.1021/op500169m.
[35] Spall, J.C. (1998). An overview of the simultaneous perturbation method for efficient optimization. *Johns Hopkins apl technical digest.* 19(4), 482-492.
[36] Yap, C.Y., Chua, C.K. & Dong, Z.L. (2016). An effective analytical model of selective laser melting. *Virtual and Physical Prototyping.* 11(1), 21-26. https://doi.org/10.1080/17452759.2015.1133217.
[37] Pawlak, A., Rosienkiewicz, M. & Chlebus, E. (2017). Design of experiments approach in AZ31 powder selective laser melting process optimization. *Archives of Civil and Mechanical Engineering.* 17, 9-18. https://doi.org/10.1016/j.acme.2016.07.007.
[38] Sun, J., Yang, Y. & Wang, D. (2013). Parametric optimization of selective laser melting for forming Ti6Al4V samples by Taguchi method. *Optics & Laser Technology.* 49, 118-124. https://doi.org/10.1016/j.optlastec.2012.12.002.
[39] Bai, Y., Yang, Y., Xiao, Z., Zhang, M. & Wang, D. (2018). Process optimization and mechanical property evolution of AlSiMg0. 75 by selective laser melting. *Materials & Design*. 140, 257-266. https://doi.org/10.1016/j.matdes.2017.11.045.
[40] Larimian, T., Kannan, M., Grzesiak, D., Al Mangour, B. & Borkar, T. (2020). Effect of energy density and scanning strategy on densification, microstructure and mechanical properties of 316L stainless steel processed via selective laser melting. *Materials Science and Engineering: A*. 770, 138455. https://doi.org/10.1016/j.msea.2019.138455.
[41] Pearson, P. & Cousins, A. (2016). Assessment of corrosion in amine-based post-combustion capture of carbon dioxide systems. *Absorption-based post-combustion capture of carbon dioxide*. 439-463. https://doi.org/10.1016/B978-0-08-100514-9.00018-4.
[42] Martin, S., Lepaumier, H., Picq, D., Kittel, J., De Bruin, T., Faraj, A. & Carrette, P.L. (2012). New amines for CO2 capture. IV. Degradation, corrosion, and quantitative structure property relationship model. *Industrial and Engineering Chemistry Research*. 51(18), 6283-6289. https://doi.org/10.1021/ie2029877.
[43] Cherry, J.A., Davies, H.M., Mehmood, S., Lavery, N.P., Brown, S.G.R., & Sienz, J. (2015). Investigation into the effect of process parameters on microstructural and physical properties of 316L stainless steel parts by selective laser melting. *The International Journal of Advanced Manufacturing Technology*. 76, 869-879. 8), 6283-6289. https://doi.org/10.1021/ie2029877.
[44] Davidson, K. & Singamneni, S. (2016). Selective laser melting of duplex stainless steel powders: an investigation. *Materials and Manufacturing Processes.* 31(12), 1543-1555. https://doi.org/10.1080/10426914.2015.1090605.
[45] Suwanpreecha, C., Seensattayawong, P., Vadhanakovint, V. & Manonukul, A. (2021). Influence of specimen layout on 17-4PH (AISI 630) alloys fabricated by low-cost additive manufacturing. *Metallurgical and Materials Transactions A*. 52, 1999-2009. https://doi.org/10.1007/s11661-021-06211-x.
[46] Dilip, J.J.S., Zhang, S., Teng, C., Zeng, K., Robinson, C., Pal, D. & Stucker, B. (2017). Influence of processing parameters on the evolution of melt pool, porosity, and microstructures in Ti-6Al-4V alloy parts fabricated by selective laser melting. *Progress in Additive Manufacturing*. 2, 157-167. https://doi.org/10.1007/s40964-017-0030-2.
[47] Tian, Y., Tomus, D., Rometsch, P. & Wu, X. (2017). Influences of processing parameters on surface roughness of Hastelloy X produced by selective laser melting. *Additive Manufacturing.* 13, 103-112. https://doi.org/10.1016/j.addma.2016.10.010.
[48] Gong, H., Rafi, K., Gu, H., Starr, T. & Stucker, B. (2014). Analysis of defect generation in Ti–6Al–4V parts made using powder bed fusion additive manufacturing processes. *Additive Manufacturing*. 1, 87-98. https://doi.org/10.1016/j.addma.2014.08.002.
[49] Wen, S., Wang, C., Zhou, Y., Duan, L., Wei, Q., Yang, S. & Shi, Y. (2019). High-density tungsten fabricated by selective laser melting: Densification, microstructure, mechanical and thermal performance. *Optics & Laser Technology*. 116, 128-138. https://doi.org/10.1016/j.optlastec.2019.03.018.
[50] Meier, H. & Haberland, C. (2008). Experimental studies on selective laser melting of metallic parts.

Materialwissenschaft und Werkstofftechnik. 39(9), 665-670. DOI: 10.1002/mawe.200800327.

[51] Garcia-Cabezon, C., Castro-Sastre, M.A., Fernandez-Abia, A.I. et al. (2022). Microstructure–hardness–corrosion performance of 17–4 precipitation hardening stainless steels processed by selective laser melting in comparison with commercial alloy. *Metals and Materials International.* 28, 2652–2667. https://doi.org/10.1007/s12540-021-01155-8.